Brain Functional Mapping Using Spatially Regularized Support Vector Machines

Xiaomu Song
Department of Electrical Engineering
School of Engineering
Widener University
Chester, PA 19013

Lawrence P. Panych
Department of Radiology
Brigham and Women's Hospital
Harvard Medical School
Boston, MA 02115

Nan-kuei Chen
Brain Imaging and Analysis Center
Duke University Medical Center
Durham, NC 27710

***Abstract*—Quantitative functional magnetic resonance imaging (fMRI) requires reliable mapping of brain function in task- or resting-state. In this work, a spatially regularized support vector machine (SVM)-based technique was proposed for brain functional mapping of individual subjects and at the group level. Unlike most SVM-based fMRI data analysis approaches that conduct supervised classifications of brain functional states or disorders, the proposed technique performs a semi-supervised learning to provide a general mapping of brain function in task- or resting-state. The method can adapt to between-session and between-subject variations of fMRI data, and provide a reliable mapping of brain function. The proposed method was evaluated using synthetic and experimental data. A comparison with independent component analysis methods was also performed using the experimental data. Experimental results indicate that the proposed method can provide a reliable mapping of brain function and be used for different quantitative fMRI studies.**

I. Introduction

Identifying brain function in a task condition or resting-state is a basic step of quantitative functional magnetic resonance imaging (fMRI) used in neuroscience studies or clinical applications. With recent advances of high field magnetic resonance imaging scanners, increased spatial resolution can be achieved in fMRI and it becomes more critical to map brain function accurately and reliably.

Existing brain mapping techniques can be categorized as model-driven and data-driven. In model-driven approaches, fMRI data are characterized by parametric models, and computed test statistics are compared to a predefined threshold to determine if a voxel is "active" or functionally "connected" [1]. In quantitative fMRI studies, multiple scan sessions are usually acquired from single or multiple subjects. A fixed model and/or threshold is often used in model-driven approaches, and this cannot adapt to variations of data characteristics between sessions and subjects [2]. Data-driven techniques do not superimpose parametric models to fMRI data, and can adapt to the changes of data characteristics. A widely used data-driven method is independent component analysis (ICA) that assumes fMRI data to be a linear combination of multiple independent sources in spatial or temporal domain [3]. A major challenge of ICA is the unknown number of underlying sources. Each obtained independent component (IC) could be a combination of multiple sources. It is also possible that a single source is divided into different ICs. Thus, a template matching or visual inspection is required to obtain meaningful mapping results [4].

In this work, a data-driven technique was developed to map brain function specific to a task stimulation or a resting-state functional network. The method integrates one-class and two-class support vector machines (SVM) together to perform a semi-supervised learning of fMRI data. SVM has been used for supervised classifications of brain functional states or disorders in task- and resting-state fMRI studies [5], [6]. Because of the between-session/subject variations of fMRI data, a trained SVM classifier may not perform well for data acquired from different sessions/subjects. Therefore, the supervised SVM-based methods were not typically used for the general mapping of brain function. It has been shown in our previous works that task- and resting-state brain functions can be identified using unsupervised/semi-supervised SVM implementations [7], [8]. Since active or functionally connected voxels are usually grouped together at multiple anatomic sites, to facilitate the mapping of the spatially grouped voxels, spatial regularization is integrated into the SVM learning in the proposed method. This method can perform functional mapping for a single slice or whole brain. It can be used to analyze task- and resting-state data for individual subjects and at the group level.

II. Proposed Method

The method was developed based upon an assumption that the number of active voxels in a task stimulation, or functionally connected voxels in a resting-state network is less than a half of the number of all voxels in brain. In this context, "outliers" denote active voxels in a task fMRI study, or functionally connected voxels in a resting-state network. Correspondingly, "majority" indicates inactive or functionally unconnected voxels. Fig. 1 shows a block diagram of the proposed method.

Motion artifacts and scanner drift are first attenuated in the preprocessing, followed by the spatial smoothing using a wavelet domain Bayesian de-noising method [9]. After the spatial smoothing, multiple features are extracted to represent each voxel and used as the input to a spatially regularized one-class SVM (SR-OCSVM). The SR-OCSVM output may

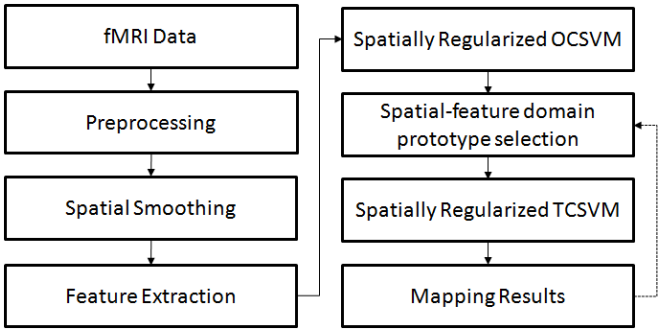

Fig. 1. The block diagram of the proposed method.

contain false detections. Thus a spatial-feature domain prototype selection is performed to select voxels that are correctly classified by SR-OCSVM. The selected voxels are used to train a spatially regularized two-class SVM (SR-TCSVM) to reclassify the input voxels. The prototype selection and SR-TCSVM reclassification may be iterated multiple times till no more change is observed in the final functional map.

A. Feature Extraction

For task fMRI data, the expected haemodynamic response (HDR) is obtained by convolving the stimulation paradigm with the canonical haemodynamic response function [1]. The following features are computed to construct a feature vector to represent each voxel: correlation coefficient (cc) value between the voxel and HDR, average, maximum, and minimum cc values between neighboring voxels of the voxel and HDR, and average signed extreme value of the cross correlation functions (ccf) between the voxel's neighboring voxels and HDR. For resting-state data, a seed is identified from a region-of-interest that is part of a functional network. The features extracted from each voxel include: cc value between the voxel and seed, average, maximum, and minimum cc values between neighboring voxels of the voxel and seed, and average cc value between the voxel and its neighboring voxels.

B. Spatially Regularized Support Vector Machines

Given a set of independent identically distributed m-dimensional data samples $x_i \in R^m$, $i = 1, \cdots n$, and their class labels y_i, the two-class SVM (TCSVM) learning aims to solve the following optimization problem [10]:

$$\min_{\mathbf{w},b,\xi} \frac{1}{2}\|\mathbf{w}\|^2 + C\sum_{i=1}^{n}\xi_i, \tag{1}$$

subject to $y_i(\langle \mathbf{w} \cdot x_i \rangle + b) \geq 1 - \xi_i$, where $\mathbf{w}$ and b define the classification hyperplane, $\xi_i \geq 0$ is the slack variable, and C controls the hyperplane complexity. As an extension of TCSVM, the one-class SVM (OCSVM) learning minimizes this objective function [11]:

$$\min_{\mathbf{w},\rho,\xi} \frac{1}{2}\|\mathbf{w}\|^2 + \frac{1}{\nu n}\sum_{i=1}^{n}\xi_i - \rho, \tag{2}$$

subject to $\langle \mathbf{w}, \Phi(\mathbf{x}_i) \rangle \geq \rho - \xi_i$, where ρ is the offset parameter, $\Phi(x_i)$ is a nonlinear mapping of $\mathbf{x}_i$, and $\nu \in (0, 1]$ represents an upper bound on the fraction of outliers. The OCSVM and TCSVM learning are specific cases of a general regularization framework [12]:

$$J(f) = \arg\min_{\mathbf{w}\in H} \frac{1}{n}\sum_{i=1}^{n} V(\mathbf{w}, \mathbf{x}_i, y_i) + \lambda_r \|\mathbf{w}\|_H^2, \tag{3}$$

where V is a loss function, H represents a reproducing kernel Hilbert space (RKHS), $\|\mathbf{w}\|_H^2$ is the norm of the classification function in H, and λ_r is a regularization parameter. The solution of (3) has a form of [13]: $f(\mathbf{x}) = \sum_{i=1}^{n} \alpha_i K(\mathbf{x}, \mathbf{x}_i)$.

If fMRI feature vectors are assumed to lie in a manifold of a high dimensional space, the brain mapping in task- or resting-state becomes a classification problem regularized by the geometry of the underlying manifold. The manifold is estimated by characterizing the spatial connectivity of neighboring voxels using a graph representation, where each voxel is represented by a vertex and connected to its surrounding voxels through edges. An adjacency matrix Θ is formed with each entry $\theta_{i,j}$ showing the connectivity strength of the edge between the i^{th} voxel and its j^{th} neighbor, and a penalty term is built as:

$$L(\mathbf{w}) = \frac{1}{nk}\sum_{i=1}^{n}\sum_{j=1}^{k}\theta_{i,j}\|f(\mathbf{x}_i) - f(\mathbf{x}_j)\|^2, \tag{4}$$

where j is the index of neighboring voxels of the i^{th} voxel. In this work, a correlation-based edge weighting is used to reflect the connectivity strength between neighboring voxels:

$$\theta_{i,j} = \frac{cc(\mathbf{x}_i, \mathbf{x}_j)}{\sum_{l=1}^{k} cc(\mathbf{x}_i, \mathbf{x}_l)}, \tag{5}$$

where $cc(\mathbf{x}_i, \mathbf{x}_j)$ is the cc value (normalized by the Fisher r-to-z transformation) between the i^{th} voxel and its j^{th} neighbor. If the spatial constraint is integrated into the SVM learning, then the regularization framework defined in (3) is modified as follows:

$$f^* = \arg\min_{\mathbf{w}\in H} \frac{1}{n}\sum_{i=1}^{n} V(\mathbf{w}, \mathbf{x}_i, y_i) + \lambda_r\|\mathbf{w}\|_H^2 + \lambda_s L(\mathbf{w}), \tag{6}$$

where λ_s is a weight parameter. The optimization of an SVM is usually performed on its dual form. Based upon the penalty term in (4), the regularized SVM learning defined in (6) can be implemented by replacing the original kernel matrix $\mathbf{K}$ with a modified kernel matrix $\tilde{\mathbf{K}}$ in the dual forms of SR-OCSVM and SR-TCSVM [14]:

$$\tilde{\mathbf{K}} = \mathbf{K} - \mathbf{K}^T(\mathbf{I} + \mathbf{M}\mathbf{K})^{-1}\mathbf{M}\mathbf{K}, \tag{7}$$

where $\mathbf{M} = \lambda_s \mathbf{L}$, and $\mathbf{L}$ is the graph Laplacian computed as $\mathbf{L} = \mathbf{D} - \mathbf{\Theta}$, and $\mathbf{D}$ is a diagonal matrix with $D_{i,i} = \sum_{j=1}^{k}\theta_{i,j}$.

The SR-OCSVM learning needs to set the parameter ν, which is task-, network-, session-, and subject-dependent, and cannot be accurately estimated. An initial estimation of ν can be obtained using the correlation analysis with Bonferroni

correction. This estimation is conservative and the estimated ν is multiplied by a factor ranging from 1.0 to 3.5. The sensitivity of the proposed method to ν was investigated in the experimental study.

After the final SR-TCSVM reclassification, SVM scores are transferred into probability estimates [15]. The final decision on each voxel is made by comparing the voxel's probabilities of "active" and "inactive" in task-state, or those of functionally "connected" and "unconnected" in resting-state. For the group level functional mapping, each voxel's probabilities of "active/connected" and "inactive/unconnected" are averaged across all subjects and sessions, and the final mapping is performed by comparing the averaged probabilities.

C. Spatial-feature Domain Prototype Selection

The feature vector representing a voxel and its class label form a prototype. In the proposed method, a prototype selection procedure is performed to identify voxels that are most possible to be correctly classified by SR-OCSVM. Using the graph representation of each voxel, if a voxel's class is the dominant class in its predefined neighborhood, then the voxel is selected as a training prototype for SR-TCSVM. To improve the representativeness of identified training prototypes, 5% of voxels in the majority and outlier classes that are closest to the SR-OCSVM classification hyperplane in the feature space are excluded from the training data because there is a higher chance for them to be mis-classified.

III. Experimental Study

A synthetic task fMRI time series was generated using a single slice echo planar imaging (EPI) image with a block design paradigm: 20 images off, 20 images on, and 20 images off. Two artificial activations were added as shown in Fig. 2 (a). The image size was 64×64. The active regions on the top left and bottom right represent 3.77% and 5.77% of the brain area, with a blood oxygen level dependent (BOLD) increase of 4% and 7% during the task period. A synthetic resting-state data was generated from another EPI image. The data consists of 100 images with four artificial functional regions, as shown in Fig. 2 (b). The image size is 120×120. Regions $1 \sim 4$ takes up 1.54%, 1.69%, 2.15% and 1.1% of the brain area, respectively. Sinusoid signals were added to regions 1 and 4 at a frequency of 0.08 Hz to form network A. The signal amplitudes of regions 1 and 4 are 107% and 104% of the baseline average, and there is a phase shift of -0.52 radians between the signals. Regions 2 and 3 form network B with sinusoidal signals added at a frequency of 0.03 Hz. The signal amplitudes are 102% and 103% of the baseline average in regions 2 and 3, respectively. The signal phase shift between the two regions is 0.78 radians. Rician noise was added to the synthetic data. After mean-centering the data, the SNR of task data is 4×10^{-4}dB, and that of resting-state data is -25.18dB.

Multiple task experimental datasets were used to evaluate the proposed technique at the individual and group levels, including three visual task and sixty six motor task datasets.

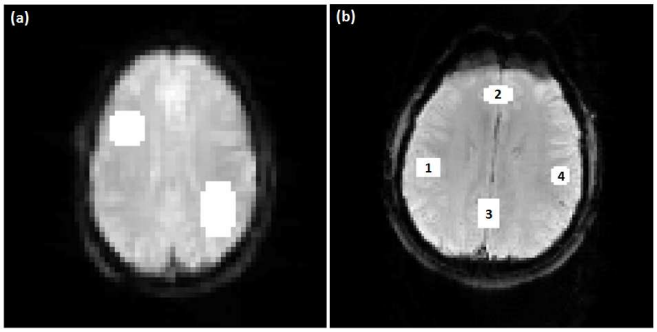

Fig. 2. (a) Synthetic task fMRI data with two active regions. (b) Synthetic resting-state fMRI data with two pairs of functionally connected regions: regions 1 and 4 are connected to form network A, and regions 2 and 3 form network B.

The visual task data are provided on the website of New York University Center for Brain Imaging (cbi.nyu.edu). They were acquired from a subject using a 3 T Siemens Allegra scanner with a repetition time (TR) of 1.5 seconds, an echo time (TE) of 30 milliseconds, and a flip angle of $70°$. A visual stimulation was used by alternatively showing a left and right circular hemifield stimulus of alternating checks at full contrast. 150 volumes were collected in each dataset with twenty five axial-slices in each volume. The image matrix size was 64×80, and spatial resolution of each isotropic voxel was $3 \times 3 \times 3\ mm^3$. The motor task data were acquired from eight subjects using a 1.5 T GE scanner at Brigham and Women's Hospital. Nine scans were performed for each subject with an inter-session gap between 21 and 140 days. In each scan, the subject was performing a right hand finger tapping task with a block design paradigm: four 30-second task blocks and five 30-second off blocks. The imaging parameters included a TR of 2.5 seconds, a TE of 50 milliseconds, and a flip angle of $90°$. Twenty four axial-slices were acquired for each volume with a slice thickness of 6 mm. The matrix size was 64×64. 114 volumes were collected in each scan, and the first 6 volumes were removed as the dummy scan, resulting in 108 volumes used in the analysis.

The proposed method was also evaluated using resting-state experimental data at the individual and group levels. In the individual level study, a dataset provided by Duke University Medical Center was used. It was collected from a subject using a 3 T GE system and a T2*-weighted parallel EPI with an acceleration factor of 2. The scan lasted 5 minutes with the following EPI parameters: TR=2 seconds, TE=25 milliseconds, and flip angle=$90°$. 35 axial-slices were acquired in each volume with a slice thickness of 3 mm. Field of view (FOV) was $24 \times 24\ cm^2$, and the image size was 64×64. The data for group level analysis were acquired from eight healthy subjects using a 1.5 T GE scanner at Brigham and Women's Hospital. Nine scans were performed for each subject, with an inter-session gap ranged from 21 to 133 days. In each scan, 24 axial-slices were acquired in each volume with 6 mm slice thickness and no gap. The imaging parameters included: TR=2.5 seconds, TE=50 milliseconds, and flip angle=$90°$. The

image size was 64×64, and the FOV was $24 \times 24\ cm^2$. 114 volumes were collected in each scan, and the first 6 volumes were removed as the dummy scan, leading to 108 volumes in each scan. Because of a computer storage failure, only 66 task datasets and 67 resting-state datasets collected at Brigham and Women's Hospital were retrievable and used in this work.

The proposed method was compared to the widely used ICA methods in the experimental study. In the study of individual subjects, the probabilistic ICA (PICA) method was used for the comparison [16]. In the PICA method, the intensity values of each IC are transferred into spatial Z-scores and a Gaussian mixture model is used to characterize the Z-scores. The final decision can be made with a probability threshold of 0.5, which is equivalent to the soft decision of the proposed method by comparing the probabilities of active/connected and inactive/unconnected voxels. In the group level study, the group ICA (GICA) was performed using the Group ICA fMRI Toolbox (GIFT) [17]. Kendall's coefficient of concordance (KCC) was also calculated to measure the regional homogeneity of active or functionally connected regions identified by the proposed and ICA methods. KCC was used with mapping results together to evaluate the mapping performance. If active or functionally connected regions are sufficiently identified, a greater KCC value indicates a better match of the identified functional regions to the true functional regions.

IV. Results

A. Synthetic Data

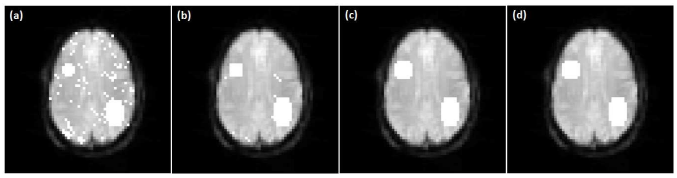

Fig. 3. Mapping results of the synthetic task data obtained using: (a) OCSVM, (b) SR-OCSVM, and the proposed method with two different ν values: (c) 0.1, (d) 0.3.

When the task synthetic data were used to evaluate SR-OCSVM, $\lambda_r = 0.01$, $\lambda_s = 0.001$, and $\nu = 0.15$. The radial basis function (RBF) kernel was used to implement a nonlinear SVM learning. Fig. 3 (a) shows the activation map obtained using the conventional OCSVM, and (b) is the SR-OCSVM result. It was observed that SR-OCSVM outperforms OCSVM. Figs. 3 (c) and (d) show the final mapping results of the synthetic task data obtained using the proposed method with (c) $\nu = 0.1$ and (d) $\nu = 0.3$. It can be seen that the mapped active regions match the ground truth very well.

When the resting-state synthetic data were used, the algorithm was set in the same way as that for the task data analysis except that $\nu = 0.1$. Figs. 4 (a)-(d) show the functional maps of network A obtained using (a) OCSVM, (b) SR-OCSVM, and the proposed method with (c) $\nu = 0.1$ and (d) $\nu = 0.3$. Figs. 4 (e)-(h) show the maps of network B obtained using the same set of methods as (a)-(d). Comparisons between (a) and (b), (e) and (f) indicate that SR-OCSVM outperforms OCSVM. It was also observed that the proposed method can provide consistent mapping results with little dependence on the setting of ν value.

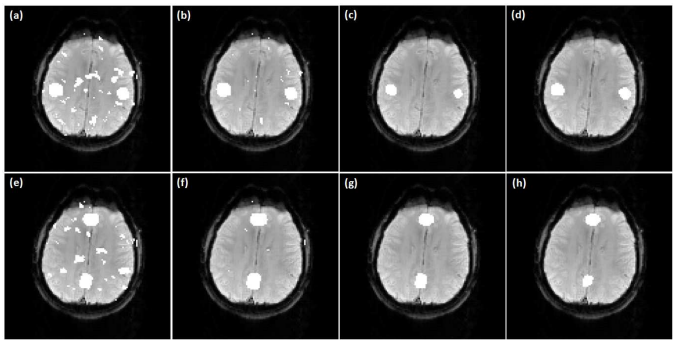

Fig. 4. Networks A and B in the synthetic resting-state data identified using: (a),(e) OCSVM, (b),(f) SR-OCSVM, and the proposed method with two different ν values: (c),(g) $\nu = 0.1$, (d),(h) $\nu = 0.3$.

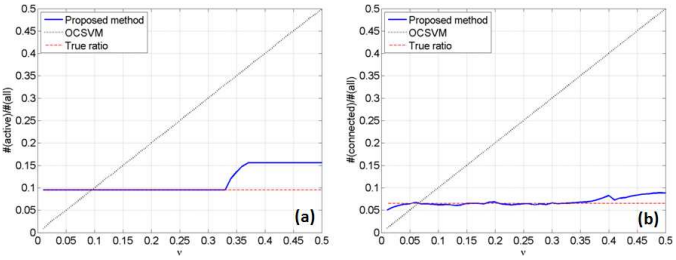

Fig. 5. Dependence of the synthetic data mapping results on ν obtained using OCSVM and the proposed method. (a) Task data. (b) Resting-state data.

Fig. 5 (a) illustrates the sensitivities of the OCSVM and proposed methods on ν, where the solid line represents the ratio of active voxels identified by the proposed method to all voxels in the brain area. The dashed line is the true ratio that is 0.0954, and the dotted line is the ratio of the OCSVM results. When ν ranges from 0.01 to 0.33, the ratio obtained from the proposed method is the same as the true ratio, and when $\nu > 0.33$, the ratio slightly increases but is much less than those obtained using OCSVM, showing less dependence on ν as compared to OCSVM. Fig. 5 (b) shows the same set of dependence patterns obtained using the synthetic resting-state data. The true ratio of networks A and B is 0.0648. The ratio obtained from the proposed method changes slightly around the true ratio when ν is between 0.01 and 0.35, and slightly increases when $\nu > 0.35$. The sensitivity of the proposed method on ν is much less than that of OCSVM.

B. Experimental Data

When analyzing the experimental fMRI data, the correlation analysis was used to provide an initial estimation of ν. Fig. 6 shows the activation maps of the visual task data, where (a)-(c) were obtained using the proposed method with three ν values: 0.11, 0.14, and 0.17, which are 2, 2.5, and 3 times the original ν value estimated from the correlation analysis. The mapping result obtained using PICA is shown in Fig. 6 (d).

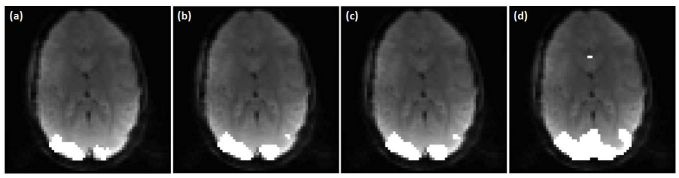

Fig. 6. (a)-(c) Activation maps of the visual task data obtained using the proposed method with ν = (a) 0.11, (b) 0.14, and (c) 0.17. (d) Activation map identified using PICA.

The regional homogeneity was calculated using active voxels identified in the left visual cortex, and the KCC values of Figs. 6 (a)-(d) are 0.215, 0.206, 0.206, and 0.157, respectively. KCC values of active voxels identified using the proposed method are higher than that from PICA.

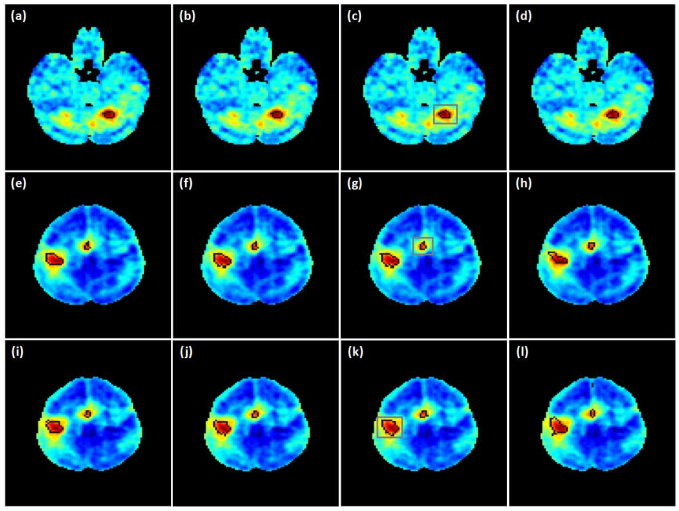

Fig. 7. Group level activation maps of the motor task data obtained using the proposed method and GICA. (a)-(c), (e)-(g), (i)-(k) The active regions in the ipsilateral cerebellar, primary/pre-motor and supplementary motor cortex areas identified by the proposed method with ν values 2.0 (a, e, i), 2.5 (b, f, j), and 3.0 (c, g, k) times the originally estimated ones. (d),(h),(l) Activation maps obtained using GICA. Dark lines denote the boundaries of the active regions. The thresholds of GICA were adjusted to identify the same numbers of active voxels in the regions encircled by the grey lines as shown in (c), (g), and (k).

In the group level study of the motor task data, both λ_r and λ_s were set to be 0.1 after testing different combinations. The active regions identified by the proposed method and GICA are shown in Fig. 7 over the average contrast-to-noise ratio (CNR) map computed using all data in the motor task experiment. Regions encircled by the dark lines in (a)-(d) are the active regions in the ipsilateral cerebellar area, where (a)-(c) were obtained using the proposed method with ν values 2.0, 2.5, and 3.0 times the estimated ones, and (d) is the GICA mapping result. A "hard" threshold is needed in GICA to identify the active regions. To make the comparison at the same mapping sensitivity level in the ipsilateral cerebellar area, the GICA threshold was adjusted to identify the same number of active voxels as that in the rectangular region encircled by the grey line as shown in Fig. 7 (c). The active regions identified by the proposed method and GICA well match the high CNR region.

Figs. 7 (e)-(h) show the mapping results from a slice partially covering the primary/pre-motor and supplementary motor cortex, where (e)-(g) were obtained using the proposed method with ν values 2.0, 2.5, and 3.0 times the originally estimated ones. The supplementary motor cortex region is encircled by the grey rectangular as shown in Fig. 7 (g), and the GICA threshold was selected to identify the same number of active voxels in this region. The boundary of the identified active region in the primary/pre-motor area is also encircled by the dark line as shown in Figs. 7 (e)-(h). The change of ν value does not lead to apparent variations in the mapping results of the proposed method. In this slice, the active regions in the supplementary motor cortex identified by the proposed and GICA methods well match the high CNR region. However, the activation in the primary/pre-motor areas mapped by the proposed method better matches the high CNR region than the GICA mapping result, as shown in Figs. 7 (g) and (h).

Figs. 7 (i)-(k) illustrate the mapping results from another slice obtained using the proposed method with ν values 2.0, 2.5, and 3.0 times the estimated ones, and (l) was obtained using GICA. The GICA threshold was set to identify the same number of active voxels as that in the rectangular region encircled by the grey line as shown in Fig. 7 (k). The active region in the supplementary motor cortex is also illustrated in each of these activation maps. The activation maps shown in Figs. 7 (i)-(k) better match the high CNR regions in the primary/pre-motor and supplementary motor cortex than those shown in (l). The KCC values of active regions in the ipsilateral cerebellar, supplementary motor cortex, and primary/pre-motor areas identified using the proposed method (as shown in Figs. 7 (c), (g), (k)) are 0.573, 0.63, and 0.417, respectively. Those of activations identified by GICA are 0.579, 0.638, and 0.403, respectively. The KCC values of active regions identified by the two methods are quite close to each other in this group study.

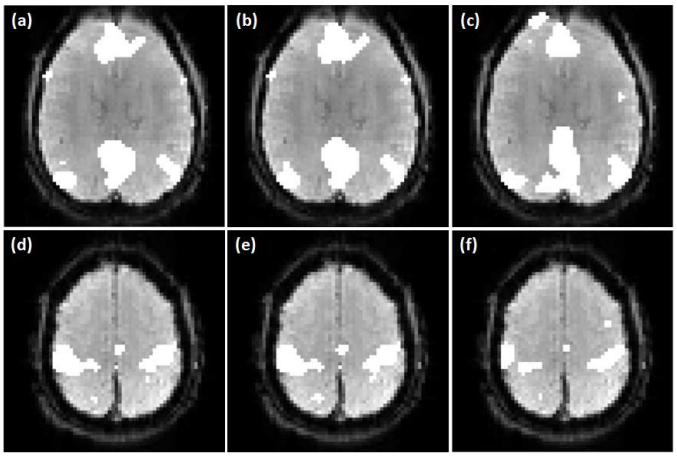

Fig. 8. (a)-(b) Part of DMN identified from an individual subject using the proposed method with two different ν values: (a) 0.27, (b) 0.41. (d)-(e) Part of SMN obtained using the proposed method with ν equal to (d) 0.25 and (e) 0.34. (c),(f) Connectivity maps obtained using PICA.

In the analysis of the individual subject's data from the resting-state experiments, the following parameters were used: $\lambda_r = 0.01$, $\lambda_s = 0.005$. Initial ν values were estimated using the correlation analysis based on a pre-selected seed. Figs. 8 (a) and (b) show part of default mode network (DMN) overlaid on an individual slice identified using the proposed method with ν = (a) 0.27 and (b) 0.41, which are 2.0 and 3.0 times the originally estimated value. Fig. 8 (c) shows the functional connectivity map obtained using PICA. The KCC values of the identified regions in (a)-(c) are 0.115, 0.118, and 0.098, respectively. Figs. 8 (d)-(f) show part of sensori-motor network (SMN) overlaid on another slice from the same subject, where (d) and (e) were obtained using the proposed method with ν = (d) 0.25 and (e) 0.34, which are 1.5 and 2.0 times the estimated one. Fig. 8 (f) shows the connectivity map obtained from PICA. The KCC values of the identified regions in (d)-(f) are 0.117, 0.121, and 0.123, respectively. The KCC values of active regions identified by the two methods are slightly different with several permillage or percentage points.

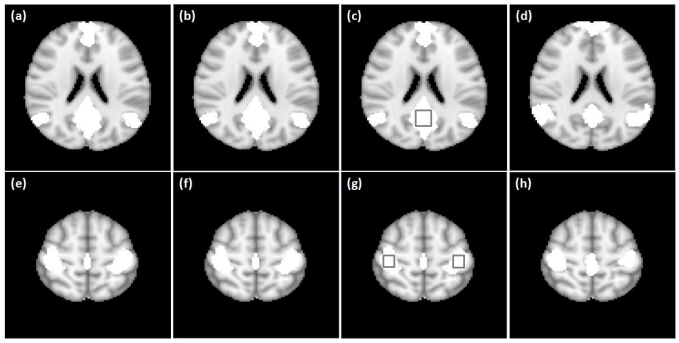

Fig. 9. (a)-(c) Part of DMN identified in the group study using the proposed method with ν equal to (a) 2.0, (b) 2.5, and (c) 3.0 times the estimated ones. (e)-(g) Part of SMN identified at the group level using the proposed method with ν equal to (e) 2.0, (f) 2.5, and (g) 3.0 times the originally estimated values. (d),(f) GICA mapping results. The thresholds of GICA were set to identify the same numbers of functionally connected voxels in the encircled regions as shown in (c) and (g).

In the group level analysis of the resting-state experimental data, the settings of λ_r and λ_s were the same as those for the group level analysis of the motor task data. Figs. 9 (a)-(c) and (e)-(g) show part of DMN and SMN mapped using the proposed method with ν equal to 2.0, 2.5, and 3 times the originally estimated values. Figs. 9 (d) and (h) show the functional connectivity maps obtained using GICA. The thresholds of GICA were adjusted to identify the same numbers of functionally connected voxels in the encircled regions as shown in Figs. 9 (c) and (g). The KCC values of functionally connected regions in DMN identified by the proposed and GICA methods (as shown in Figs. 9 (c) and (d)) are 0.21 and 0.18, respectively. Those in SMN mapped by the proposed and GICA methods (as shown in Figs. 9 (g) and (h)) are 0.28 and 0.27, respectively. It can be seen that the functionally connected regions in DMN and SMN identified by the proposed method have slightly higher regional homogeneity than those mapped by GICA.

V. Conclusion

In this work, a spatially regularized SVM technique was developed to map brain function in task conditions and resting-state. The method combines OCSVM and TCSVM to perform a semi-supervised learning to adapt to the between-session and between-subject variations of fMRI data. Spatial regularization is integrated into the OCSVM and TCSVM learning to facilitate the identification of spatially grouped functional regions. The method was evaluated based upon a comparison with the widely used ICA methods at the individual and group levels. Experimental results indicate that the proposed technique outperforms the ICA methods and can provide a reliable mapping of brain function in task- and resting-state.

References

[1] K. Friston, A. Holmes, and et al., "Statistical parametric maps in functional imaging: a general linear approach," *Hum. Brain Mapp.*, vol. 2, pp. 189–210, 1995.

[2] C. Genovese, N. Lazar, and T. Nichols, "Thresholding of statistical maps in functional neuroimaging using the false discovery rate," *NeuroImage*, vol. 15, pp. 870–878, 2002.

[3] V. Calhoun, T. Adali, G. Pearlson, and J. Pekar, "Spatial and temporal independent component analysis of functional MRI data containing a pair of block-design waveforms," *Hum. Brain Mapp.*, vol. 13, pp. 43–53, 2001.

[4] V. Schöpf, C. Kasess, and et al., "Fully exploratory network ICA (FENICA) on resting-state fMRI data," *J Neurosci Methods*, vol. 192, pp. 207–213, 2010.

[5] D. Cox and R. Savoy, "Functional magnetic resonance imaging (fMRI) "brain reading": detecting and classifying distributed patterns of fMRI activity in human visual cortex," *NeuroImage*, vol. 19, pp. 261–270, 2003.

[6] R. Craddock, P. H. III, and et al., "Disease state predication from resting state functional connectivity," *Magn Reson Med*, vol. 62, pp. 1619–1628, 2009.

[7] X. Song and A. Wyrwicz, "Unsupervised spatiotemporal fMRI data analysis using support vector machines," *NeuroImage*, vol. 47, pp. 204–212, 2009.

[8] X. Song and N.-K. Chen, "A SVM-based quantitative fMRI method for resting-state functional network detection," *Magn. Reson. Imaging*, vol. 32, pp. 819–831, 2014.

[9] X. Song, M. Murphy, and A. Wyrwicz, "Spatiotemporal denoising and clustering of fMRI data," in *Proc. IEEE Int. Conf. Image Process.*, 2006, pp. 2857–2860.

[10] V. N. Vapnik, *Statistical learning theory*. Wiley-Interscience, 1998.

[11] B. Schölkopf, J. Platt, and et al., "Estimating the support of high-dimensional distribution," *Neural Comput.*, vol. 13, no. 7, pp. 1443–1471, 2001.

[12] M. Belkin, P. Niyogi, and V. Sindhwani, "Manifold regularization: a geometric framework for learning from labeled and unlabeled examples," *Journal of Machine Learning Research*, vol. 7, pp. 2399–2434, 2006.

[13] B. Schölkopf, R. Herbrich, and A. Smola, "A generalized representer theorem. computational learning theory," *Lecture Notes in Computer Science*, vol. 2111, pp. 416–426, 2001.

[14] V. Sindhwani, P. Niyogi, and M. Belkin, "Beyond the point cloud: from transductive to semi-supervised learning," in *Proc. the 22nd Intl. Conf. Machine Learning*, 2005, pp. 824–831.

[15] T. Wu, C. Lin, and R. Weng, "Probability estimates for multi-class classification by pairwise coupling," *J Mach Learn Res.*, vol. 5, pp. 975–1005, 2004.

[16] C. Beckmann and S. Smith, "Probabilistic independent component analysis for functional magnetic resonance imaging," *IEEE Trans. Medical Imaging*, vol. 23, no. 2, pp. 137–152, 2004.

[17] V. Calhoun, J. Liu, and T. Adali, "A review of group ICA for fMRI data and ICA for joint inference of imaging, genetic, and ERP data," *NeuroImage*, vol. 45, no. 1 Suppl, pp. S163–S172, 2009.